Elastic coupling power stroke mechanism of the F_1-ATPase molecular motor

James L. Martin[a], Robert Ishmukhametov[a,1], David Spetzler[a,2], Tassilo Hornung[a,2], and Wayne D. Frasch[a,3]

[a]School of Life Sciences, Arizona State University, Tempe, AZ 85287

Edited by Martin Karplus, Harvard University, Cambridge, MA, and approved April 16, 2018 (received for review February 21, 2018)

The angular velocity profile of the 120° F_1-ATPase power stroke was resolved as a function of temperature from 16.3 to 44.6 °C using a $\Delta\mu_{ATP} = -31.25\ k_BT$ at a time resolution of 10 μs. Angular velocities during the first 60° of the power stroke (phase 1) varied inversely with temperature, resulting in negative activation energies with a parabolic dependence. This is direct evidence that phase 1 rotation derives from elastic energy (spring constant, $\kappa = 50\ k_BT{\cdot}rad^{-2}$). Phase 2 of the power stroke had an enthalpic component indicating that additional energy input occurred to enable the γ-subunit to overcome energy stored by the spring after rotating beyond its 34° equilibrium position. The correlation between the probability distribution of ATP binding to the empty catalytic site and the negative E_a values of the power stroke during phase 1 suggests that this additional energy is derived from the binding of ATP to the empty catalytic site. A second torsion spring ($\kappa = 150\ k_BT{\cdot}rad^{-2}$; equilibrium position, 90°) was also evident that mitigated the enthalpic cost of phase 2 rotation. The maximum $\Delta G^{\ddagger}$ was 22.6 k_BT, and maximum efficiency was 72%. An elastic coupling mechanism is proposed that uses the coiled-coil domain of the γ-subunit rotor as a torsion spring during phase 1, and then as a crankshaft driven by ATP-binding–dependent conformational changes during phase 2 to drive the power stroke.

F_1-ATPase | F-type ATP synthase | single molecule | F_OF_1 ATP synthase | power stroke mechanism

In living organisms, the majority of cellular ATP is synthesized from ADP and phosphate (Pi) by the F_OF_1 ATP synthase (1). The F_1 complex is a rotary molecular motor powered by ATPase activity and is composed of an axle (minimally the γ-subunit) that rotates within its $(\alpha\beta)_3$-ring stator (Fig. 1*A*). The $(\alpha\beta)_3$-ring, with a catalytic site located on each β-subunit (Fig. 1*B*), surrounds the γ-subunit coiled-coil domain. The adjacent γ-"foot" domain docks to the ring of c-subunits in F_o. The membrane-embedded F_o motor uses a nonequilibrium transmembrane ion gradient (usually H^+) as an energy source to rotate the c-ring in the opposite direction from that powered by the F_1 motor. This results in the synthesis of ATP at the three F_1 catalytic sites. Since each c-subunit in the c-ring translocates one proton across the membrane, the organism-dependent variation of the c_{8-16}-ring (2) is rarely an integer multiple of the three F_1 catalytic sites. However, the γ-subunit coiled-coil has sufficient compliance to accommodate these stoichiometric disparities (3, 4).

The β-subunit contains a catalytic domain that includes the P-loop where the nucleotide Mg^{2+}-phosphoryl complex binds and hydrolysis occurs, and a helical domain that binds to the nucleotide base via π−π stacking with aromatic groups. The distal end of this latter "lever" domain engages the γ-subunit coiled-coil and changes conformation to a closed position upon the binding of nucleotide. In F_1 crystal structures (5), the γ-subunit foot domain is positioned above a β-subunit designated β_T that contains bound ATP, or ATP analog (*SI Appendix*, Fig. S1), while the second and third sites typically contain no nucleotide (β_E), and bound ADP (β_D).

When powered by the F_1-ATPase, the γ-subunit completes one rotation in three successive 120° counterclockwise (CCW) power strokes, each separated by a catalytic dwell (4, 6–9). Catalytic dwells are rate-limiting to ATPase activity, and occur on a 2- to 7-ms timescale (8, 10) that is much longer than ∼300-μs power strokes (6). During a typical catalytic dwell, one site (β_T) contains tightly bound ATP, the second site (β_D) hydrolyzes its bound ATP, and the third (β_E) becomes empty upon release of product Pi (8, 11, 12). The incidence and duration of a second dwell during the first 60° of the power stroke increases inversely with ATP concentration when substrate limits the overall rate of the enzyme (6, 8, 13). The distribution of rotary positions of this ATP-binding dwell, which results from ATP binding to β_E, is closely similar to dwells that result from ADP product inhibition. In addition to the competition of ADP with ATP for the binding to β_E, elevated ADP concentrations slow the release of ADP formed at β_D during a catalytic dwell, which slows rotation throughout the power stroke (6).

Relative to the level of understanding of events that occur during dwells, little is understood about the mechanism that causes the γ-subunit to revolve between dwells (the power stroke). Torque values of about 40 and 60 pN·nm have been measured for *Gs*F_1 (14) and *Ec*F_1 (4, 15), from *Geobacillus stearothermophilus* (formally *Bacillus* PS3) and *Escherichia coli*, respectively, under conditions in which drag on the visible probe limits the average rate of rotation. Previous investigations concluded that *Gs*F_1 operates with 100% efficiency relative to the chemical potential of ATP hydrolysis (14, 16–19). The claim of 100% efficiency is based on the ratio of useful work to the free energy of ATP hydrolysis, where useful work is defined as the

Significance

Molecular motor F_1-ATPases use the free energy from ATP binding and hydrolysis to ADP and Pi to rotate subunit γ, and can synthesize ATP in the F_OF_1 ATP synthase. We determined the energetics during each 3° of the power stroke from temperature-dependent changes of angular velocity. Unexpectedly, the power stroke activation energy of phase 1 (0°–60°) was negative and varied parabolically, indicating that it was powered by elastic energy of a torsional spring consistent with unwinding the γ-subunit coiled-coil. Phase 2 rotation had an enthalpic component, indicating additional input of energy is required to complete the 120° power stroke, consistent with energy derived from ATP binding. These results deepen our understanding of these important molecular motors summarized in the proposed elastic coupling mechanism.

Author contributions: D.S. and W.D.F. designed research; J.L.M., R.I., D.S., and T.H. performed research; J.L.M. and W.D.F. analyzed data; and J.L.M. and W.D.F. wrote the paper.

The authors declare no conflict of interest.

This article is a PNAS Direct Submission.

[1]Present address: Department of Physics, University of Oxford, Oxford OX1 3PJ, United Kingdom.

[2]Present address: Caris Life Sciences, Phoenix, AZ 85040.

[3]To whom correspondence should be addressed. Email: frasch@asu.edu.

This article contains supporting information online at www.pnas.org/lookup/suppl/doi:10.1073/pnas.1803147115/-/DCSupplemental.

Published online May 14, 2018.

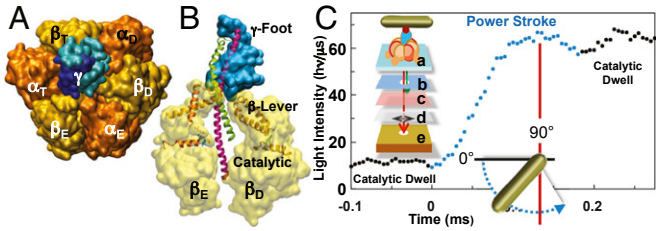

Fig. 1. F_1-ATPase single-molecule rotation assay. (*A*) F_1-ATPase (PDB entry 1E79) view from membrane. (*B*) Cross-section of F_1 with β_E and β_D lever and catalytic domains, and γ–coiled-coil (green, pink) and foot (cyan) domains. (*C*) Light intensity from a nanorod versus time during an F_1 power stroke with 1 mM Mg^{2+} and 2 mM ATP (●). Polarizer was aligned perpendicular to the nanorod during preceding catalytic dwell (●). Nanorod angular position relative to polarizer is shown with 0°:90° as min:max light intensities. (*Inset*) Schematic for measurements where (a) F_1 was attached to a Ni-coated slide by 6×His tags on β-subunit C termini, and to a 75 × 35-nm streptavidin-coated gold nanorod via specific γ-subunit biotinylation. Light scattered from the nanorod passed through a (b) pinhole; (c) bandpass filter to exclude all but red light; (d) polarizing filter; then collected by (e) avalanche photodiode sampled at 200 kHz.

average angular velocity during the power stroke against an opposing force. The efficiency of molecular motors, including F_1, are known to increase when working against near-stall forces (20). As thermodynamic efficiency increases, the extent of free energy dissipation (entropy creation) decreases (21). The ability of ATP hydrolysis to contribute directly to the ∼300-μs γ-subunit power stroke is thought to be unlikely (22), since the dissipation of energy in proteins from such an exothermic reaction occurs in picoseconds (23). However, the relative binding energies of ATP, ADP, and Pi to F_1 can provide a significant source of energy to power rotation (22, 24–26).

Measurements of the γ-subunit power stroke with a time resolution of 10 μs and high precision of the angular position revealed that the angular velocity proceeds through a series of specific angle-dependent accelerations and decelerations under conditions in which drag on the visible probe is not rate limiting (6, 27). ATP binding occurs during accelerations and decelerations in the first 60° after the catalytic dwell, designated phase 1. The phase 2 (60°–120°) acceleration/deceleration profile correlated well with the profile derived from molecular dynamics (MD) simulations that modeled subunit-γ rotation in response to ATP-binding induced closure of the β-subunit lever acting on subunit γ as a cam (6, 25). This supports a mechanism where changes in β-subunit conformation act on subunit γ through repulsive van der Waals interactions to drive rotation. Alternatively, other MD simulations predict that electrostatic interactions are predominantly responsible for subunit-γ rotation (28), and another model proposes that elastic energy in subunit γ is used to drive rotation during the power stroke in a Brownian ratchet-type mechanism (29).

We now report the effects of temperature on the angular velocity profile of the *Ec*F_1 (hereafter F_1) power stroke resolved at a time resolution of 10 μs. The power stroke angular velocity varied inversely with temperature during phase 1, resulting in negative activation energy (E_a) values that provide direct evidence that elastic energy drives rotation during phase 1. A switch then occurs such that phase 2 rotation has an enthalpic component, indicating an additional input of energy occurs for the phase 2 power stroke.

Results

Power stroke velocities from single molecules of F_1 were measured using changes in polarized red light intensity scattered from a gold nanorod attached to subunit γ that was rotating in the presence of 2 mM Mg^{2+} and 1 mM ATP (Fig. 1*C*). The viscous drag of these nanorods was determined not to limit the rate of F_1-ATPase–driven rotation (7, 15). Sinusoidal intensity changes of scattered polarized red light increase from minimum to maximum as the long axis of the nanorod rotates from perpendicular to parallel with the polarizing filter. Rotation of each F_1 molecule was recorded with a single photon detector in 5-s datasets at 200 kHz after rotating the polarizing filter to minimize scattered light intensity during one catalytic dwell (30). The 120° power stroke subsequent to this catalytic dwell caused the intensity to increase from a minimum through a maximum, at which point the γ-subunit had rotated 90°, and then to decrease until the next catalytic dwell began (Fig. 1*C*). The light intensity data from these power strokes were collected, and the rotational position as a function of time was calculated (*SI Appendix*, Fig. S2) using an $\arcsin^{1/2}$ function (27).

Rotation datasets from single F_1 molecules were collected at temperatures from 16.3 to 44.6 °C. The *Ec*F_1-ATPase is thought to remain stable over this range since Årrhenius plots of ensemble ATPase measurements remain linear at 55 °C (31, 32). Using a pyruvate kinase/lactic dehydrogenase-coupled assay, the ADP concentration in the rotation assay was determined to be 10 μM, which, with an equivalent Pi concentration, resulted in a $\Delta\mu_{ATP}$ of −31.25 k_BT. At these concentrations, the F_1-ATPase operates at k_{cat} with minimal product inhibition.

The angular velocity of subunit γ versus rotational position from the end of the catalytic dwell (Fig. 2*A*) was determined for each power stroke via changes in the slope of each of three consecutive data points in a running average. Angular velocities at each rotational position were averaged and binned for each 3° of rotation. At all temperatures examined, the angular velocity profiles contained a similar pattern of accelerations and decelerations as a function of rotational position to those reported previously (6, 27) and differed from each other only in the magnitude of angular velocities at various rotary positions.

All Årrhenius plots from the angular velocities at each 3° position fit to linear functions (*SI Appendix*, Fig. S2) like those

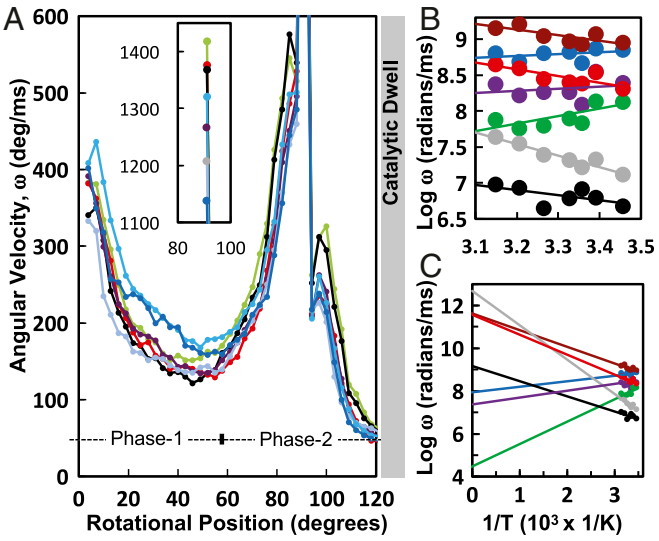

Fig. 2. Effects of temperature on F_1-ATPase–driven γ-subunit power stroke angular velocities versus rotational position. (*A*) Angular velocities measured at temperatures in degrees Celsius of 16.3° (●), 22.0° (●), 24.8° (●), 27.6° (●), 33.3° (●), 38.9° (●), and 44.6° (●), calculated using 3,522, 6,675, 3,987, 4,518, 4,383, 2,358, and 4,362 total power strokes from 24, 39, 30, 33, 39, 15, and 21 F_1 molecules. Data were binned every 3° of rotation from the end of the catalytic dwell. (*Inset*) Angular velocities at the 88° rotary position. (*B* and *C*) Årrhenius analyses of F_1-ATPase–driven power stroke angular velocity at rotational positions of 4° (●), 16° (●), 37° (●), 76° (●), 85° (●), 109° (●), and 121° (●).

shown at rotational positions 4°, 16°, 37°, 76°, 85°, 109°, and 121° (Fig. 2 *B* and *C*), supporting the conclusion that the F_1-ATPase was stable over this temperature range. Unexpectedly, the angular velocity changed inversely with temperature during most of the first 60° of rotation after the catalytic dwell. As a result, the activation energy (E_a) values derived from these Arrhenius plots were negative during phase 1 of the power stroke and reached a minimum of −3.5 k_BT at ∼34° after the catalytic dwell (Fig. 3*A*). As rotation continued after 34°, E_a increased versus rotational position such that it was zero at 61°, at which point the angular velocity did not change significantly as a function of temperature. The E_a continued to increase during phase 2 of the power stroke, reaching the first maximum of 4.3 k_BT at 79° when subunit-γ rotation was accelerating. At 88°, E_a reached a local minimum of 1.3 k_BT, and then increased again to a maximum of 7.5 k_BT at 106° during the final deceleration as subunit γ approached the next catalytic dwell.

Negative E_a values indicate that the energy used for the work for phase 1 rotation is of entropic origin, which is characteristic of elastic energy (33, 34), and is commonly observed in long biological polymers like protein coiled-coils (35, 36). Twisting a coiled-coil away from its equilibrium position stores elastic energy that can serve as an entropic spring capable of mechanical work when it unwinds (37). This is believed to occur because fewer conformations are possible when a coiled-coil is twisted, which reduces the entropy significantly (38). Allowing a coiled-coil to return to its untwisted equilibrium position exerts a restoring force as the number of possible conformations, and the associated entropy, increase.

Assuming that the negative E_a values resulted only from compliance of subunit γ, the torsional elastic modulus (κ) during phase 1 was determined by fitting the negative E_a values to the following: $U = 1/2(\kappa\phi^2)$, where U is the amount of stored potential energy as a function of ϕ, the angle of twist of the γ-subunit from its equilibrium position in radians. Using the equilibrium position of 34° where E_a reached a minimum value, the best fit of the data in Fig. 3*A* was achieved with a torsional elastic modulus of 50 $k_BT{\cdot}rad^{-2}$ (205 $pN{\cdot}nm{\cdot}rad^{-2}$, red curve). The values of E_a between 79° and 106° that had a local minimum at 88° were also fit to a plot of energy stored in a torsion spring (green curve) that fit best with $\kappa = 150\ k_BT{\cdot}rad^{-2}$.

The relationship of the phase 1 power stroke elastic energy dependence to the rotary position at which ATP binds to the empty catalytic site was determined from ATP-binding dwells that occurred during power strokes collected in the presence of 0.3 mM Mg-ATP as per examples in *SI Appendix*, Fig. S4. The resulting probability distribution of ATP-binding dwells (Fig. 3, *Inset*) occurred primarily between phase 1 rotary positions 9°–60° with a maximum at ∼34°. This distribution is comparable (*SI Appendix*, Fig. S5) to that reported for GsF_1 (8). It is noteworthy that the inverse of the probability distribution of the ATP-binding dwells correlates well with the negative E_a values observed during phase 1 of the power stroke (Fig. 3). The fit to the ATP-binding dwell data (red curve) is the same as that derived using a 50 $k_BT{\cdot}rad^{-2}$ spring constant. Thus, the changes in protein conformation that result from elastic energy correlate well with the ability of ATP to bind to the empty catalytic site.

The free energy of activation ($\Delta G^{\ddagger}$) profile of the F_1-ATPase power stroke and its enthalpic ($\Delta H^{\ddagger}$) and entropic ($T\Delta S^{\ddagger}$) components were derived from the Arrhenius analysis. The enthalpy of activation that is proportional to E_a was also negative during phase 1 of the power stroke (Fig. 3*B*). The free energy of activation (Fig. 3*C*), determined from $\Delta G^{\ddagger} = \Delta H^{\ddagger} - T\Delta S^{\ddagger}$, was positive throughout the power stroke because it was dominated by $T\Delta S^{\ddagger}$ (Fig. 3*B*). The profile of $\Delta G^{\ddagger}$ versus rotational position was inversely proportional to the angular velocity of subunit γ during the power stroke (Fig. 3*C*). Although this is not particularly evident from inspection of the $\Delta H^{\ddagger}$ and $T\Delta S^{\ddagger}$ profiles, it does make physical sense in that higher angular velocities correspond to lower free energy of activation barriers.

In addition to the power stroke, the process of ATPase-driven rotation of subunit γ includes the catalytic dwell. Literature values of the catalytic dwell thermodynamic parameters are shown as open symbols in Fig. 3. During the catalytic dwell, ATP hydrolysis occurs before Pi release, which starts the power stroke. The $\Delta G^{\ddagger}$ for ATP hydrolysis (□) derived from GsF_1-ATPase single-molecule studies (39) was comparable to what we observed at the end of the power stroke, when it transitions to the catalytic dwell (Fig. 3*C*). The GsF_1-ATPase $\Delta G^{\ddagger}$ for Pi release (Δ) is only slightly higher than our value at the start of the power stroke, which is also consistent. Although $\Delta G^{\ddagger}$ values of Pi release and ATP hydrolysis correspond to those at the start and end of the power stroke, respectively, the $\Delta H^{\ddagger}$ and $T\Delta S^{\ddagger}$ values from which they were derived (Fig. 3*B*) are significantly higher than those that define the power stroke. This suggests that the underlying processes during the catalytic dwell and power stroke differ substantially.

Discussion

Results presented here provide key insights into the rotary mechanism of the F_1-ATPase as a function of rotational position during the power stroke. First, negative E_a values during the first 60° of rotation indicate that the energy for phase 1 of the power stroke is derived from elastic energy with a spring constant of ∼50 $k_BT{\cdot}rad^{-2}$. Thus, when the catalytic dwell ends, rotation is powered by the unwinding of a torsion spring that reaches its

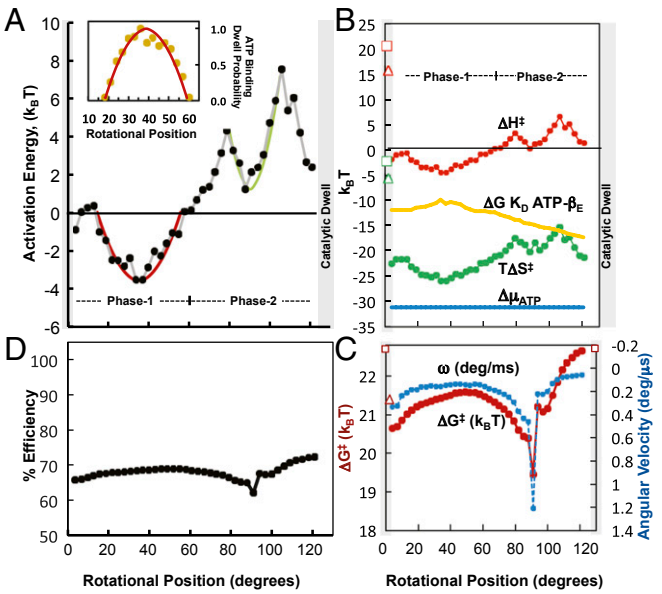

Fig. 3. Thermodynamic values at 298 K of F_1-ATPase–driven power stroke angular velocities. (*A*) Activation energy (●) during power strokes versus rotational position. Energy stored as a function of the extent of twist of a torsion spring with a spring constant, $\kappa = 50\ k_BT{\cdot}rad^{-2}$ (—) and 150 $k_BT{\cdot}rad^{-2}$ (—) from equilibrium positions of 34° and 88°, respectively. (*Inset*) Probability ATP-binding dwell formation with 0.3 mM MgATP (●) from *SI Appendix*, Figs. S3 and S4. Fit of data to the inverse of energy stored from twist of a $\kappa = 50\ k_BT{\cdot}rad^{-2}$ torsional spring and 34° equilibrium position (—). (*B*) Enthalpy of activation, $\Delta H^{\ddagger}$ (●), and energy dissipation, $T\Delta S^{\ddagger}$ (●). Chemical energy, $\Delta\mu_{ATP}$ (— —), was determined from [ATP], [ADP], and [Pi] present during measurements. The free energy for ATP binding to the empty catalytic site, $\Delta G\ K_D$-ATP (— —), determined from K_D for GsF_1-ATPase (46). (*C*) Free energy of activation, $\Delta G^{\ddagger}$ (●), and the angular velocity of the power stroke, ω (●). Catalytic dwell values for Pi release (△), and for ATP hydrolysis (□) using GsF_1-ATPase (39). (*D*) F_1-ATPase–driven power stroke efficiency versus rotational position was determined from $-\Delta G^{\ddagger}/\Delta\mu_{ATP}$.

equilibrium position at 34°. The CCW rotation continues with negative E_a values 34°–60°, but increasingly at the expense of winding the spring beyond the equilibrium position. Second, a switch occurs 60° into the power stroke such that phase 2 of the power stroke has an enthalpic component. This indicates that additional energy input occurred to enable subunit γ to overcome the energy stored by the spring at rotary positions 34°–60° for continued rotation during phase 2. However, in phase 2, the entropic contribution is still larger than that from enthalpy. Third, the close correlation between the probability distribution of ATP binding to the empty catalytic site and the negative E_a values of the power stroke during phase 1 suggests that this additional energy input is derived from the binding affinity of ATP. Fourth, the ATP-binding dwell can occur throughout phase 1 with a maximal probability at 34°, contrary to previous reports that ATP binds specifically at 40° (8).

These conclusions are incorporated into the elastic coupling mechanism (Fig. 4). As the catalytic dwell ends (Fig. 4*A*), catalytic site β_D hydrolyzed ATP to Pi and ADP. Behind subunit γ, catalytic site β_T (not pictured) has bound ATP. Lacking bound nucleotide, the β_E lever domain is in the open conformation. Several F_1 structures have similar nucleotide occupancy with some variability of β_E-bound Pi (5, 40–45). In eubacterial F_1, the catalytic dwell is thought to end upon Pi release from β_E (12). This initiates phase 1 of the power stroke (Fig. 4*B*), which derives its energy to rotate from a torsion spring that reaches equilibrium at 34° (Fig. 3*A*). Subunit-γ rotation acts as a camshaft on the β-lever domains, which behave as cam followers during phase 1. This alters the distance between the lever and catalytic domains that bind the adenine ring and the phosphoryl groups of ATP, respectively, which can explain the dependence of nucleotide binding affinity on rotary position (46). The ATP binding energy derives from attractive forces of the adenine base via π–π stacking with aromatic residues in the β-lever domain, and from electrostatic attraction between the Mg(II)-phosphoryl complex of the ATP to the P-loop of the β-catalytic domain (47). While ATP binding to β_E can occur at any rotary position during phase 1, it is most probable at 34° when E_a reaches its minimum (Fig. 3*A*, *Inset*), consistent with MD simulations that show that the highest probability of forming the ATP-binding dwell occurs at an energy minimum (48).

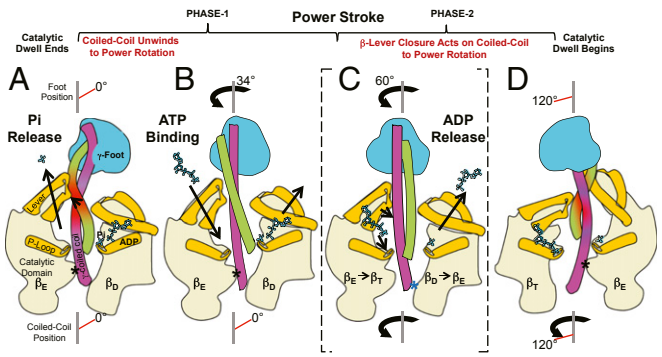

Fig. 4. Elastic coupling mechanism of the F_1-ATPase power stroke. (*A*) Catalytic dwell (0°) after ATP hydrolysis at β_D. Tightly wound γ–coiled-coil and $(\alpha\beta)_3$-ring are tethered (✱). Power stroke starts by β_E-Pi release to allow coiled-coil unwinding. (*B*) Phase 1 rotation (0°–60°): γ–coiled-coil torsion spring unwinds to equilibrium γ-foot domain position of 34°. β_E binds ATP at any phase 1 rotational position, 34° is optimal. β_D dissociates ADP optimally at 34° but can slow phase 2 if delayed. (*C*) Phase 1 → phase 2 switch at 60° when the γ–coiled-coil reaches the winding limit. Electrostatic interactions between Mg-ATP and groups on the β_E lever and catalytic domains force conformational changes to break γ–coiled-coil tether and push β_E lever against subunit γ to rotate foot and coiled-coil. A different tether (✱) may cause a second spring (80°–100°). (*D*) Catalytic dwell begins when γ-foot reaches 120°, and β-subunit conformations change ($\beta_E \rightarrow \beta_T$ and $\beta_D \rightarrow \beta_E$). ATP hydrolysis rewinds torsion spring.

Phase 2 of the power stroke (Fig. 4*C*) is thought to result from force applied to subunit γ as a crankshaft from ATP binding-dependent closure β_E-lever (i.e., the lever moves subunit γ) (6, 25). This is supported by the fit of the angular velocity profile of the power stroke during phase 2 that estimated the potential energy coupling of the action of the β-subunit levers on the γ-subunit calculated via targeted MD trajectories. This energy input enables subunit γ to rotate beyond the 60° winding limit of the phase 1 torsional spring. This is characteristic of a power stroke-dependent process (49), which contradicts assertions that F_1 operates solely by a Brownian ratchet mechanism (50).

At β_D, the ADP binding affinity also changes as a function of γ-rotational position. Elevated ADP concentrations have been shown to slow phase 2 of the power stroke (6), which is postulated to result from delayed dissociation of ADP necessary to open the β_D-lever. This was minimized by the very low ADP concentrations used here. Catalytic site conformations change (β_E to β_T, β_D to β_E, and β_T to β_D) during phase 2. During the subsequent catalytic dwell (Fig. 4*D*), ATP hydrolysis occurs at the newly formed β_D, and the torsion spring that provides elastic energy for phase 1 of the next power stroke must become rewound.

We hypothesize that the torsion spring responsible for phase 1 of the power stroke results primarily from changes in the extent of winding of the γ-subunit coiled-coil domain. This is illustrated using images of 1H8E for Fig. 4 *A* and *D*, and of 4ASU for Fig. 4*B* that were simplified from *SI Appendix*, Fig. S1 to emphasize mechanistic features. Several observations support this relationship. The rotary position of the γ-foot domain varies among crystal structures by as much as 43° such that this domain in Protein Data Bank (PDB) entries 2JDI and 4ASU (51, 52) are CCW of PDB entry 1H8E (53) by 13° and 39°, respectively (*SI Appendix*, Fig. S1*C*). Based on catalytic site occupancy and rotary position of the γ-foot, 2JDI and 4ASU are considered catalytic dwell and ATP-binding dwell conformations, respectively. To behave as a torsional spring, the γ–coiled-coil must be tethered to the $(\alpha\beta)_3$-ring at some location (Fig. 4, ✱) to enable tight winding that can store elastic energy. In all F_1 structures known to date, subunit γ is tethered to the $(\alpha\beta)_3$-ring by electrostatic interactions that include the β_E "catch loop" (β_EE302, β_ED305) and the C-terminal end of the γ–coiled-coil (γR256L, γQ257) that are distal from the foot domain (5, 40–45). Due to these interactions, the coiled-coil varies from tightly (PDB entry 1H8E) to loosely (PDB entries 4ASU and 3OAA) wound. Single-site mutations β_EE302T, β_ED305E, and γR256L that weaken the β_E-catch loop/γ-subunit electrostatic interactions dramatically decrease ATPase activity (31). Additional γ-subunit/$(\alpha\beta)_3$-ring interactions (28, 32, 54–58) may also contribute to the F_1-ATPase mechanism (✱). Our results are consistent with studies that show that truncation of subunit γ significantly decreases rotation rate. Mutations that cumulatively shorten the length of the shaft decrease rotation speed, leading Furuike et al. (59) to conclude that the γ–coiled-coil has a crucial role in the rotary mechanism. Truncating as few as 8 and 29 of the 60 N-terminal helix residues decreased the rotation rate and ATPase activity by 50% and 85%, respectively, while truncating a segment of the C-terminal helix that eliminates interaction with the β_E catch loop decreases the rotation rate by 50% (60, 61).

The torsional moduli of 50 and 150 $k_BT{\cdot}rad^{-2}$ observed here are higher than that determined for compliance of the γ–coiled-coil measured by cross-linking experiments (3), and as calculated from chemomechanical group transfer theory (62). However, spatial heterogeneity of rotary fluctuations that were identified by atomistic simulations of the F_1 torsional elasticity, were modeled into a set of eight harmonically coupled segments of the γ-subunit in conjunction with the $(\alpha\beta)_3$-ring (63). Of these, two pairs of harmonically coupled coiled-coil segments were calculated to have spring constants of 85 and 134 $k_BT{\cdot}rad^{-2}$,

respectively, which were closest to the experimentally derived values reported here. These γ–coiled-coil segments correspond to locations within F_1 in which the β-subunit catch-loop and lever domains interact with the γ-subunit, consistent with the elastic coupling mechanism (Fig. 4).

The presence of tethers between subunit γ and the $(\alpha\beta)_3$-ring was observed at three rotary positions when a magnetic particle attached to the γ-subunit was forced to rotate by an external magnet (16). Forced rotation caused subunit γ to behave as a torsion spring with equilibrium positions at three successive rotary locations. The equilibrium positions of the torsional springs observed here in phase 1 and phase 2 are at the same rotary locations as the springs designated I and II, respectively, observed by Saita et al. (16). While the use of magnetic force to control the rotational position of subunit γ revealed the existence of torsional springs, the limits imposed by the magnetic force eliminate the ability to determine the contributions of these springs to the mechanism of the power stroke.

The Årrhenius analysis presented here was performed under conditions in which the ATP concentration was not rate limiting such that the occurrence of ATP-binding dwells was insignificant. The concentrations of ADP and Pi were also low enough to minimize product inhibition such that $\Delta\mu_{ATP}$ was $-31.25\ k_BT$ (Fig. 3*B*). For a process, here the power stroke, to overcome its energy barrier and proceed to rotate past a given rotational position, the output energy must exceed $\Delta G^{\ddagger}$, the free energy of activation (20). During the power stroke $\Delta G^{\ddagger} < -31.25\ k_BT$, reaching a maximum of $22.6\ k_BT$ at 120°, the start of the catalytic dwell. The efficiency of the motor calculated from the ratio of $-\Delta G^{\ddagger}/\Delta\mu_{ATP}$ (Fig. 3*D*) ranges from 62 to a maximum of 72% at 120°. Previous investigations concluded that GsF_1 operates with 100% efficiency (14, 16–19, 64–66). This high efficiency was based on calculations of the ratio of useful work to $\Delta\mu_{ATP}$ where useful work is defined as the average angular velocity during the power stroke against a rate-limiting opposing force. The efficiency calculated here that was determined under conditions in which the velocity of rotation was not limited by a significant opposing force. Operating at against a near-stall force is known to increase efficiency of molecular motors including F_1 (20).

The processes of ATP binding, and of ADP and Pi dissociation from F_1 can each contribute energy for rotation. The free energy of ATP binding to the GsF_1-ATPase (Fig. 3*B*) was determined from the ATP association constant when subunit-γ rotational position was tightly controlled by a strong external magnetic force (46). The rotational position with the highest probability of binding ATP correlates with the lowest binding energy. Binding energy increases at subsequent rotary positions consistent with closure of the lever, until it reaches a maximum at the next catalytic dwell when ATP is tightly bound (β_T conformation) with a fully closed lever. Free-energy values derived from ADP and Pi dissociation can also be calculated from the data of Adachi et al. (46). These values represent an upper limit of the energy available to F_1 for rotation because the magnet held subunit γ at each rotational position for long periods required for the binding/dissociation of ATP, ADP, and Pi to reach equilibrium (46). This likely explains the smooth dependence the K_D-ATP versus rotary position (Fig. 3*B*). In contrast, conditions of the single-molecule experiments presented here allowed subunit γ to rotate at its natural unencumbered speed. Given the angular velocities reported in Fig. 2, it is likely that the catalytic sites rarely have sufficient time for substrate and product binding and dissociation to reach equilibrium at any given rotational position during the power stroke. For any given power stroke, the energy available from binding/dissociation of ATP, ADP, and Pi will depend upon the rotary position at which each occurs, and the subsequent span of rotary positions over which it contributes, which are as yet undetermined.

An Årrhenius analysis provides information regarding the energetics of the rate-limiting step in a kinetic process. For the F_1-ATPase power strokes presented here, it provided information regarding the energy barrier that limits the rate of rotation for each 3° rotary position between catalytic dwells. At each position, this limit is defined by the energy available to enable rotation, and the drag imposed by the stator as the rotating γ-subunit encounters steric and/or electrostatic obstacles on the inner surface of the $(\alpha\beta)_3$-ring. For any given power stroke, these obstacles depend on variations in the conformations of the three catalytic sites that result from the probabilities in substrate/product occupancies at these sites as a function of rotational position. Consequently, the elastic coupling mechanism proposed here does not imply tight coupling between the conformational changes of the $(\alpha\beta)_3$-ring and the rotational position of subunit γ. The observation that power strokes proceed despite the occurrence of an ATP-binding dwell that can occur over a 60° span of rotational positions (Fig. 3) is evidence of loose coupling.

The compliance of subunit γ is also important to accommodate the disparities in stoichiometry between F_o and F_1 in a manner that allows flexible power transmission during ATP synthesis (3, 4). Due to the c_{10}-ring in EcF_OF_1, H^+ translocation will power c-ring rotation 144° once (three c-subunits), and 108° twice to enable the three 120° F_1 steps that each yield ATP against an unfavorable ATP/ADP·Pi chemical gradient (67, 68). Elastic energy stored by torsion on the γ–coiled-coil during an F_1 catalytic dwell is likely to contribute to, or retard the ability to make ATP depending on the direction and extent to which the coiled-coil is wound during each dwell. This may explain the differences in the ability of single c-subunit stepping observed in single-molecule F_OF_1 experiments (69).

Methods

Slides prepared with functionalized F_1 molecules were equilibrated at each temperature by flowing water through a custom-made stage that was regulated by a water bath with positive heating and cooling control, and monitored on the slide with a thermocouple. Individual gold nanorods were initially identified to undergo F_1-ATPase–dependent rotation by observing oscillations in light intensity through a polarizing filter via a Zeiss HSC Color CCD camera at 55 fps. Each molecule observed was aligned confocal to a Perkin-Elmer SPCM-AQR-15 single photon detector (APD) to quantitate changes in scattered light intensity from the nanorods as a function of time through the acquisition of 5-s datasets at 200 kHz (30). Observation of sinusoidal dependence of the intensity positions of the three catalytic dwells as a function of the rotary position of the polarizer was used as evidence of F_1-ATPase dependent rotation of a nanorod (27, 70). Power strokes were identified by identifying light intensity fluctuations that changed from a minimum intensity defined by the lowest fifth percentile of data intensities to a maximum defined the highest fifth percentile intensities. Power stroke intensities were then converted into rotational position using the arcsine$^{1/2}$ equations as reported previously (27). The F_1-ATPase was purified from *E. coli* XL-10 strain. F_1 contains a His_6-tag on the N terminus of the α-subunit and γS193C for biotinylation as described previously (6). To biotinylate the enzyme, 200 μL of F_1 solution was mixed with equimolar amounts of biotin-maleimide and passed through a desalting column equilibrated with Wash Buffer. Biotinylated F_1 was stored at 0.1 mg/mL at –80 °C before use. Single-molecule rotation assays were performed as described previously (6).

ACKNOWLEDGMENTS. This project was supported by Grant R01GM097510 (to W.D.F.).

1. Spetzler D, et al. (2012) Energy transduction by the two molecular motors of the F_1F_o ATP synthase. *Photosynthesis: Plastid Biology, Energy Conversion and Carbon Assimilation*, Advances in Photosynthesis and Respiration, eds Eaton-Rye JJ, Tripathy BC, Sharkey TD (Springer, Dordrecht, The Netherlands), pp 561–590.
2. Pogoryelov D, et al. (2012) Engineering rotor ring stoichiometries in the ATP synthase. *Proc Natl Acad Sci USA* 109:E1599–E1608.
3. Sielaff H, et al. (2008) Domain compliance and elastic power transmission in rotary F_OF_1-ATPase. *Proc Natl Acad Sci USA* 105:17760–17765.

4. Junge W, Sielaff H, Engelbrecht S (2009) Torque generation and elastic power transmission in the rotary F_OF_1-ATPase. *Nature* 459:364–370.
5. Abrahams JP, Leslie AG, Lutter R, Walker JE (1994) Structure at 2.8 Å resolution of F_1-ATPase from bovine heart mitochondria. *Nature* 370:621–628.
6. Martin JL, Ishmukhametov R, Hornung T, Ahmad Z, Frasch WD (2014) Anatomy of F_1-ATPase powered rotation. *Proc Natl Acad Sci USA* 111:3715–3720.
7. Spetzler D, et al. (2006) Microsecond time scale rotation measurements of single F_1-ATPase molecules. *Biochemistry* 45:3117–3124.
8. Yasuda R, Noji H, Yoshida M, Kinosita K, Jr, Itoh H (2001) Resolution of distinct rotational substeps by submillisecond kinetic analysis of F_1-ATPase. *Nature* 410:898–904.
9. Hirono-Hara Y, et al. (2001) Pause and rotation of F_1-ATPase during catalysis. *Proc Natl Acad Sci USA* 98:13649–13654.
10. Spetzler D, et al. (2009) Single molecule measurements of F_1-ATPase reveal an interdependence between the power stroke and the dwell duration. *Biochemistry* 48: 7979–7985.
11. Adachi K, et al. (2007) Coupling of rotation and catalysis in F_1-ATPase revealed by single-molecule imaging and manipulation. *Cell* 130:309–321.
12. Watanabe R, Iino R, Noji H (2010) Phosphate release in F_1-ATPase catalytic cycle follows ADP release. *Nat Chem Biol* 6:814–820.
13. Sielaff H, Rennekamp H, Engelbrecht S, Junge W (2008) Functional halt positions of rotary F_OF_1-ATPase correlated with crystal structures. *Biophys J* 95:4979–4987.
14. Yasuda R, Noji H, Kinosita K, Jr, Yoshida M (1998) F_1-ATPase is a highly efficient molecular motor that rotates with discrete 120 degree steps. *Cell* 93:1117–1124.
15. Hornung T, Ishmukhametov R, Spetzler D, Martin J, Frasch WD (2008) Determination of torque generation from the power stroke of *Escherichia coli* F_1-ATPase. *Biochim Biophys Acta* 1777:579–582.
16. Saita E, Suzuki T, Kinosita K, Jr, Yoshida M (2015) Simple mechanism whereby the F_1-ATPase motor rotates with near-perfect chemomechanical energy conversion. *Proc Natl Acad Sci USA* 112:9626–9631.
17. Toyabe S, Watanabe-Nakayama T, Okamoto T, Kudo S, Muneyuki E (2011) Thermodynamic efficiency and mechanochemical coupling of F_1-ATPase. *Proc Natl Acad Sci USA* 108:17951–17956.
18. Kinosita K, Jr, Yasuda R, Noji H, Adachi K (2000) A rotary molecular motor that can work at near 100% efficiency. *Philos Trans R Soc Lond B Biol Sci* 355:473–489.
19. Kawaguchi K, Sasa S, Sagawa T (2014) Nonequilibrium dissipation-free transport in F_1-ATPase and the thermodynamic role of asymmetric allosterism. *Biophys J* 106: 2450–2457.
20. Bustamante C, Chemla YR, Forde NR, Izhaky D (2004) Mechanical processes in biochemistry. *Annu Rev Biochem* 73:705–748.
21. Chapman B, Loiselle D (2016) Thermodynamics and kinetics of the F_oF_1-ATPase: Application of the probability isotherm. *R Soc Open Sci* 3:150379.
22. Yang W, Gao YQ, Cui Q, Ma J, Karplus M (2003) The missing link between thermodynamics and structure in F_1-ATPase. *Proc Natl Acad Sci USA* 100:874–879.
23. Henry ER, Eaton WA, Hochstrasser RM (1986) Molecular dynamics simulations of cooling in laser-excited heme proteins. *Proc Natl Acad Sci USA* 83:8982–8986.
24. Gao YQ, Yang W, Marcus RA, Karplus M (2003) A model for the cooperative free energy transduction and kinetics of ATP hydrolysis by F_1-ATPase. *Proc Natl Acad Sci USA* 100:11339–11344.
25. Pu J, Karplus M (2008) How subunit coupling produces the gamma-subunit rotary motion in F_1-ATPase. *Proc Natl Acad Sci USA* 105:1192–1197.
26. Senior AE, Nadanaciva S, Weber J (2002) The molecular mechanism of ATP synthesis by F_1F_0-ATP synthase. *Biochim Biophys Acta* 1553:188–211.
27. Sielaff H, et al. (2016) Power stroke angular velocity profiles of archaeal A-ATP synthase versus thermophilic and mesophilic F-ATP synthase molecular motors. *J Biol Chem* 291:25351–25363.
28. Mukherjee S, Warshel A (2015) Dissecting the role of the γ-subunit in the rotary-chemical coupling and torque generation of F_1-ATPase. *Proc Natl Acad Sci USA* 112: 2746–2751.
29. Kulish O, Wright AD, Terentjev EM (2016) F_1 rotary motor of ATP synthase is driven by the torsionally-asymmetric drive shaft. *Sci Rep* 6:28180.
30. Hornung T, Martin J, Spetzler D, Ishmukhametov R, Frasch WD (2011) Microsecond resolution of single-molecule rotation catalyzed by molecular motors. *Methods Mol Biol* 778:273–289.
31. Greene MD, Frasch WD (2003) Interactions among gamma R268, gamma Q269, and the beta subunit catch loop of *Escherichia coli* F_1-ATPase are important for catalytic activity. *J Biol Chem* 278:51594–51598.
32. Boltz KW, Frasch WD (2005) Interactions of gamma T273 and gamma E275 with the beta subunit PSAV segment that links the gamma subunit to the catalytic site Walker homology B aspartate are important to the function of *Escherichia coli* F_1F_0 ATP synthase. *Biochemistry* 44:9497–9506.
33. Mark JE, Eisenberg A, Graessley WW, Mandelkern L, Koenig JL (1993) *Physical Properties of Polymers* (Am Chem Soc, Washington, DC), 2nd Ed.
34. Bustamante C, Marko JF, Siggia ED, Smith S (1994) Entropic elasticity of lambda-phage DNA. *Science* 265:1599–1600.
35. Neukirch S, Goriely A, Hausrath AC (2008) Chirality of coiled coils: Elasticity matters. *Phys Rev Lett* 100:038105.
36. Wolgemuth CW, Sun SX (2006) Elasticity of alpha-helical coiled coils. *Phys Rev Lett* 97: 248101.
37. Panyukov S, Rabin Y (2000) Thermal fluctuations of elastic filaments with spontaneous curvature and torsion. *Phys Rev Lett* 85:2404–2407.
38. Treloar LRG (1975) *The Physics of Rubber Elasticity* (Oxford Univ Press, London).
39. Watanabe R, Minagawa Y, Noji H (2014) Thermodynamic analysis of F_1-ATPase rotary catalysis using high-speed imaging. *Protein Sci* 23:1773–1779.
40. Bowler MW, Montgomery MG, Leslie AG, Walker JE (2006) How azide inhibits ATP hydrolysis by the F-ATPases. *Proc Natl Acad Sci USA* 103:8646–8649.
41. Rees DM, Leslie AG, Walker JE (2009) The structure of the membrane extrinsic region of bovine ATP synthase. *Proc Natl Acad Sci USA* 106:21597–21601.
42. Menz RI, Leslie AG, Walker JE (2001) The structure and nucleotide occupancy of bovine mitochondrial F_1-ATPase are not influenced by crystallisation at high concentrations of nucleotide. *FEBS Lett* 494:11–14.
43. Braig K, Menz RI, Montgomery MG, Leslie AG, Walker JE (2000) Structure of bovine mitochondrial F_1-ATPase inhibited by Mg^{2+} ADP and aluminium fluoride. *Structure* 8: 567–573.
44. Orriss GL, Leslie AG, Braig K, Walker JE (1998) Bovine F_1-ATPase covalently inhibited with 4-chloro-7-nitrobenzofurazan: The structure provides further support for a rotary catalytic mechanism. *Structure* 6:831–837.
45. Abrahams JP, et al. (1996) The structure of bovine F_1-ATPase complexed with the peptide antibiotic efrapeptin. *Proc Natl Acad Sci USA* 93:9420–9424.
46. Adachi K, Oiwa K, Yoshida M, Nishizaka T, Kinosita K, Jr (2012) Controlled rotation of the F_1-ATPase reveals differential and continuous binding changes for ATP synthesis. *Nat Commun* 3:1022.
47. Singharoy A, Chipot C, Moradi M, Schulten K (2017) Chemomechanical coupling in hexameric protein-protein interfaces harness energy within V-type ATPases. *J Am Chem Soc* 139:293–310.
48. Nam K, Pu J, Karplus M (2014) Trapping the ATP binding state leads to a detailed understanding of the F_1-ATPase mechanism. *Proc Natl Acad Sci USA* 111:17851–17856.
49. Hwang W, Lang MJ (2009) Mechanical design of translocating motor proteins. *Cell Biochem Biophys* 54:11–22.
50. Astumian RD, Mukherjee S, Warshel A (2016) The physics and physical chemistry of molecular machines. *ChemPhysChem* 17:1719–1741.
51. Bowler MW, Montgomery MG, Leslie AG, Walker JE (2007) Ground state structure of F_1-ATPase from bovine heart mitochondria at 1.9 Å resolution. *J Biol Chem* 282: 14238–14242.
52. Rees DM, Montgomery MG, Leslie AG, Walker JE (2012) Structural evidence of a new catalytic intermediate in the pathway of ATP hydrolysis by F_1-ATPase from bovine heart mitochondria. *Proc Natl Acad Sci USA* 109:11139–11143.
53. Menz RI, Walker JE, Leslie AG (2001) Structure of bovine mitochondrial F_1-ATPase with nucleotide bound to all three catalytic sites: Implications for the mechanism of rotary catalysis. *Cell* 106:331–341.
54. Mukherjee S, Bora RP, Warshel A (2015) Torque, chemistry and efficiency in molecular motors: A study of the rotary-chemical coupling in F_1-ATPase. *Q Rev Biophys* 48: 395–403.
55. Boltz KW, Frasch WD (2006) Hydrogen bonds between the alpha and beta subunits of the F_1-ATPase allow communication between the catalytic site and the interface of the beta catch loop and the gamma subunit. *Biochemistry* 45:11190–11199.
56. Lowry DS, Frasch WD (2005) Interactions between beta D372 and gamma subunit N-terminus residues gamma K9 and gamma S12 are important to catalytic activity catalyzed by *Escherichia coli* F_1F_0-ATP synthase. *Biochemistry* 44:7275–7281.
57. Nakamoto RK, Maeda M, Futai M (1993) The gamma subunit of the *Escherichia coli* ATP synthase. Mutations in the carboxyl-terminal region restore energy coupling to the amino-terminal mutant gamma Met-23→Lys. *J Biol Chem* 268:867–872.
58. Sekiya M, Nakamoto RK, Nakanishi-Matsui M, Futai M (2012) Binding of phytopolyphenol piceatannol disrupts β/γ subunit interactions and rate-limiting step of steady-state rotational catalysis in *Escherichia coli* F_1-ATPase. *J Biol Chem* 287:22771–22780.
59. Furuike S, et al. (2008) Axle-less F_1-ATPase rotates in the correct direction. *Science* 319: 955–958.
60. Hossain MD, et al. (2008) Neither helix in the coiled coil region of the axle of F_1-ATPase plays a significant role in torque production. *Biophys J* 95:4837–4844.
61. Kohori A, et al. (2011) Torque generation in F_1-ATPase devoid of the entire amino-terminal helix of the rotor that fills half of the stator orifice. *Biophys J* 101:188–195.
62. Volkán-Kacsó S, Marcus RA (2015) Theory for rates, equilibrium constants, and Brønsted slopes in F_1-ATPase single molecule imaging experiments. *Proc Natl Acad Sci USA* 112:14230–14235.
63. Czub J, Grubmüller H (2011) Torsional elasticity and energetics of F_1-ATPase. *Proc Natl Acad Sci USA* 108:7408–7413.
64. Kinosita K, Jr, Yasuda R, Noji H (2000) F_1-ATPase: A highly efficient rotary ATP machine. *Essays Biochem* 35:3–18.
65. Masaike T, et al. (2000) Rotation of F_1-ATPase and the hinge residues of the beta subunit. *J Exp Biol* 203:1–8.
66. Toyabe S, et al. (2010) Nonequilibrium energetics of a single F_1-ATPase molecule. *Phys Rev Lett* 104:198103.
67. Ishmukhametov R, Hornung T, Spetzler D, Frasch WD (2010) Direct observation of stepped proteolipid ring rotation in *E. coli* F_oF_1-ATP synthase. *EMBO J* 29:3911–3923.
68. Martin J, Hudson J, Hornung T, Frasch WD (2015) F_o-driven rotation in the ATP synthase direction against the force of F_1 ATPase in the F_oF_1 ATP synthase. *J Biol Chem* 290:10717–10728.
69. Yanagisawa S, Frasch WD (2017) Protonation-dependent stepped rotation of the F-type ATP synthase c-ring observed by single-molecule measurements. *J Biol Chem* 292: 17093–17100.
70. Ragunathan P, et al. (2017) The uniqueness of subunit α of mycobacterial F-ATP synthases: An evolutionary variant for niche adaptation. *J Biol Chem* 292: 11262–11279.